Macromolecules
ARTICLE

Macromolecules **2010**, *43*, 7549–7555 **7549**
DOI: 10.1021/ma101328p

Lyotropic Hexagonal Ordering in Aqueous Media by Conjugated Hairy-Rod Supramolecules

Shanju Zhang, Lisa D. Pfefferle, and Chinedum O. Osuji*

Department of Chemical Engineering, Yale University, New Haven, Connecticut 06511

Received June 15, 2010; Revised Manuscript Received July 27, 2010

ABSTRACT: We report on a series of experiments on hydrogels formed by supramolecular hairy-rod conjugated polymers and their lyotropic liquid crystalline behavior. The system is an ionic complex between negatively charged poly[2-(3-thienyl)ethyloxy-4-butylsulfonate)] backbones and cationic cetrimonium side chains. These hairy-rod supramolecules form stable isotropic solutions under dilute conditions with enhanced photoluminescence relative to the neat polymer itself. The system displays an isotropic-liquid crystalline transition on increasing concentration, resulting in the formation of a hexagonally ordered lyotropic mesophase in which the polymer chains are packed into hexagonally ordered rod-like assemblies. The mesophase is thermosensitive and can be isotropized by moderate heating. Although theoretically predicted, the observation of such lyotropic mesophases in conjugated polymers has not been reported to date. The results here are rationalized in terms of the uncharacteristically long side chains and inherent polydispersity of the system which appear necessary for stabilization of this mesophase. These results may provide new routes for the fabrication of well ordered conjugated polymer films from such solution ordered precursors for high performance electro-optic devices.

Introduction

Conjugated organic polymers are promising candidates for flexible opto-electronic devices such as light-emitting diodes (LEDs),[1−4] thin film transistors (TFTs),[5−7] and photovoltaics (PVs),[8−10] because of their unique combination of polymer flexibility and semiconducting electrical properties. One major attraction of conjugated polymers is their industrially viable solution-based printing and coating. However, this class of polymers is in general infusible and insoluble in common organic solvents due to their rigid backbone. Most common methods for improving their processability are based on chemical modifications by covalent linkage of flexible side chains to the polymer backbone.[11−13] The resultant hairy-rod polymers are then fusible and soluble in the common solvents. An alternative to this approach is to use physical matching interactions such as ionic or hydrogen bonding to fabricate hairy-rod supramolecules.[14−16] One distinct advantage of this supramolecular route is that the surfactant or small side-chain can be removed after processing, thus producing pristine materials.

In the melt state, hairy-rod conjugated polymers can form thermotropic liquid crystalline (LC) phases due to microphase separation between the hair-like side chains and the rod-like backbone. Theoretical calculations[17,18] and experimental studies[19−21] have shown a rich liquid crystalline phase behavior with the display of nematic, lamellar and hexagonal phases. Phase stability is a function not just of temperature, but also of the volume fraction of the side chains as well as interactions between the side chains and the polymer backbone. Thermotropic liquid crystallinity of hairy-rod conjugated polymers is of value in device engineering as it provides not only anisotropic opto-electronic properties[21−23] but also enhancement of efficient charge transport.[24,25]

In solution, hairy-rod conjugated polymers behave like rodlike particles.[26] In general, conjugated polymers tend to aggregate into large micrometer-scale clusters in solution due to $\pi-\pi$ stacking interactions.[27] Aggregates grow continually until saturation of the $\pi-\pi$ stacking interaction. Percolation of these sticky aggregates leads to the formation of a viscoelastic gel. Several investigations have also been reported in which the gelation process of hairy-rod conjugated polymers was closely associated with changes in the polymer conformation.[28−30] In this framework, interactions between the solvent and polymer play a crucial role in triggering gelation. While theoretical calculations[31−33] have shown that similarly rich liquid crystalline behavior is possible in solution as in the melt, only low ordered nematic phases have been observed experimentally in solutions of semiflexible conjugated polymers. To date, the lyotropic nematic phase has been reported in several hairy-rod conjugated polymers, including polyfluorenes (PFs),[34] poly(*p*-phenylene) (PPP),[35] phenylenevinylenes (PPVs),[36] poly(diacetylenes),[37] and poly(phenylene ethynylenes) (PPEs).[38] Using external forces such as shear flow and electric fields, aligned thin films could be obtained from the lyotropic nematic phase.[29] In general, lyotropic liquid crystallinity provides a promising route for fabricating oriented thin films during solution-based processing.[39,40] Such oriented semiconducting polymer films possess many attractive properties such as polarized electro-luminscence[41,42] and enhanced charge mobility in polymer field-effect transistors.[43] The use of higher ordered mesophases can be expected to yield improved order in the thin solid films formed from solution processing. However, to the best of our knowledge, there are no reports of highly ordered lyotropic columnar phases of conjugated polymers to date.

Here, we report on the novel display of a highly ordered lyotropic columnar phase of hairy-rod supramolecules of poly(alkyl thiophenes) in water. The hairy-rod complex is formed via ionic bond attachment of a cationic surfactant, cetrimonium bromide (CTAB) to the poly(alkylthiophene), poly[2-(3-thienyl)-ethyloxy-4-butylsulfonate)] (PTEBS) (Scheme 1). PTEBS is a recently developed water-soluble variant of the semiconducting polymer poly(alkyl thiophene), with interesting potential for

*Corresponding author. E-mail: Chinedum.Osuji@yale.edu.

Published on Web 08/17/2010

Scheme 1. (a) Model of Hairy-Rod Supramolecules of the Conjugated Polymer, (b) Chemical Structures of the Conjugated Polymer and Surfactant, and (c) Hexagonal Columnar Packing in the Lyotropic Phase[a]

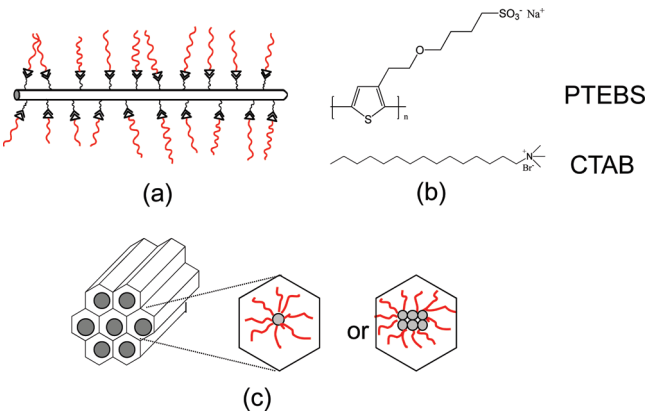

[a] A simplified two-dimensional cartoon shows two possible configurations in the hexagonal phase in which the polymer backbone is normal to the drawing plane.

clean or green processing in the manufacture of various devices.[44] The steric interactions of densely attached side chains in the complex result in a stretched backbone conformation. The supramolecule overall approaches a cylindrical form, yielding a liquid crystalline phase as is typical for such polymers in concentrated solution. Surprisingly, however, the phase displays hexagonal packing of the polymer backbones. The stabilization of the hexagonal or columnar phase may be due to the long side chains employed, and the polydispersity intrinsic to the system as these factors similarly drive the emergence of hexagonal order in melt systems.[14] We demonstrate that mechanical shearing in the liquid crystalline phase produces aligned thin films of the conjugated polymer.

Experimental Section

Sodium poly[2-(3-thienyl)ethyloxy-4-butylsulfonate)] (PTEBS) with $M_w \sim 10^6$ (American Dye Source) and cetrimonium bromide (CTAB, Aldrich) were used as received. Stock solutions (2.5×10^{-2} M) of the polymer (molar concentration is with respect to the sulfonated thiophene repeat unit) and surfactant were prepared in ultrapure water (Milli-Q, 18 MΩ). Samples of lower concentrations were obtained by dilution of the stock solutions. The complexes were prepared by dropwise addition of the surfactant solution into the polymer aqueous solution under stirring. The resultant complexes were separated by centrifugation at a speed of 14 500 rpm (14 000 g) for 30 min (Eppendorf MiniSpin Microcentrifuge).

FTIR vibration spectra were recorded on a Bruker Tensor 27 spectrometer equipped with a temperature-controlled Pike Si-crystal ATR cell. Samples were prepared by temperature controlled solvent evaporation directly on the cell to ensure good conformal contact of the polymer film with the Si-crystal. UV−vis absorption spectra were taken on Cary-100 spectrophotometer at 25 °C. The fluorescence spectra were recorded on an SLM spectrofluorometer using 400 nm excitation. Thermal properties were characterized by differential scanning calorimetry (DSC Q-200, TA Instruments) under a nitrogen flow. Optical textures were studied under cross-polarizers on a Zeiss Axiovert 200 M optical microscope equipped with a hot-stage with temperature control of ±0.5 °C (Linkam, TMS 94). Small and wide-angle X-ray scattering (SAXS, WAXS) experiments were performed on a pinhole collimated Rigaku instrument (SMAX3000) using 1.5405 Å Cu Kα radiation produced by a microfocus source. Scattering was recorded using a gas-wire electronic area (2D) detector. The scattering vector q is defined as $q = (4\pi/\theta)\sin\theta$, where 2θ is the scattering angle. The sample−detector distance was ca. 83 cm permitting access to a range of scattering vectors from 0.016 to 0.3 Å^{-1}. Calibration was performed using silver behenate with a d-spacing of 58.38 Å. Temperature dependent measurements were performed using the same hot stage utilized for polarized optical microscopy (POM). Samples were subjected to a heating/cooling rate of 5 °C/min held at the acquisition temperatures for 10 min prior to data collection.

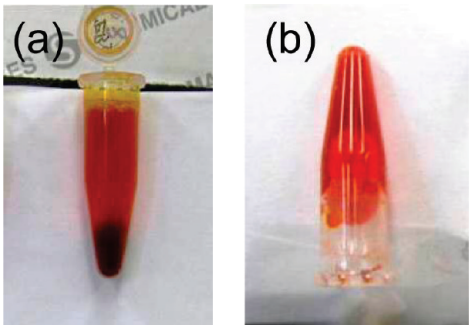

Figure 1. Photos of the gels of the PTEBS-CTAB complex: (a) three layers after centrifuge; (b) the middle layer gel.

Results and Discussion

Both the charged conjugated polymer PTEBS and the cationic surfactant CTAB are water-soluble species. Drop-wise addition of the CTAB solution into the PTEBS solution under stirring resulted in a turbid mixture. Centrifugation of the suspension produced three distinct layers as shown in Figure 1a. The top layer is a light yellow fluid, the middle layer is an orange jelly like solution, and the bottom layer is a deep red color with a mud-like consistency. This phase separation upon centrifuging is attributed to the broad polydispersity of the commercially sourced material used in this work whereby high molecular weight fractions drop out of solution before lower molecular weight ones. Such macroscopic phase separations have been well recognized in the solutions of rigid-rod liquid crystalline polymers[45,46] and also recently discovered in the solutions of carbon nanotubes.[47−49] In this work, we focus on structures and phase transitions of the middle gel-like layer (Figure 1b).

Figure 2 shows the UV−vis absorption spectra of the PTEBS aqueous solution (1×10^{-4} M) in the presence of various amounts of the CTAB. The pure PTEBS in water exhibited a broad absorption at 460 nm. Addition of CTAB resulted in a shift of the absorption maximum toward lower wavelengths, indicative of the formation of the PTEBS-CTAB ionic complex.[50] This effect saturates for CTAB concentrations greater than about 8% (molar ratio), although the CTAB continues to form complexes with the polymer and indeed does not show any macrophase separation from the polymer over all compositions studied. Evidently, there is a decoupling of the electro-optical properties from the composition of the complex beyond a critical stoichiometry. The formation of the complex is also attended by a significant decrease in the absorption intensity. The blue shift in the absorption spectra is attributed to the inhibition of polymer chain aggregation due to the incorporation of the alkyl side chains. Support along this line is also provided by the photoluminescence (PL) spectra of the complex (Figure 2b). The addition of 1 mol % CTAB to the PTEBS solution results in enhancement of the PL emission, or a suppression of photoquenching. This is again indicative of a dissolution of aggregates or inhibition of aggregation due to the incorporation of the side chains.[51] Similar observations have been reported for polythiophene/polyfluorene based polymers and copolymers.[52,53]

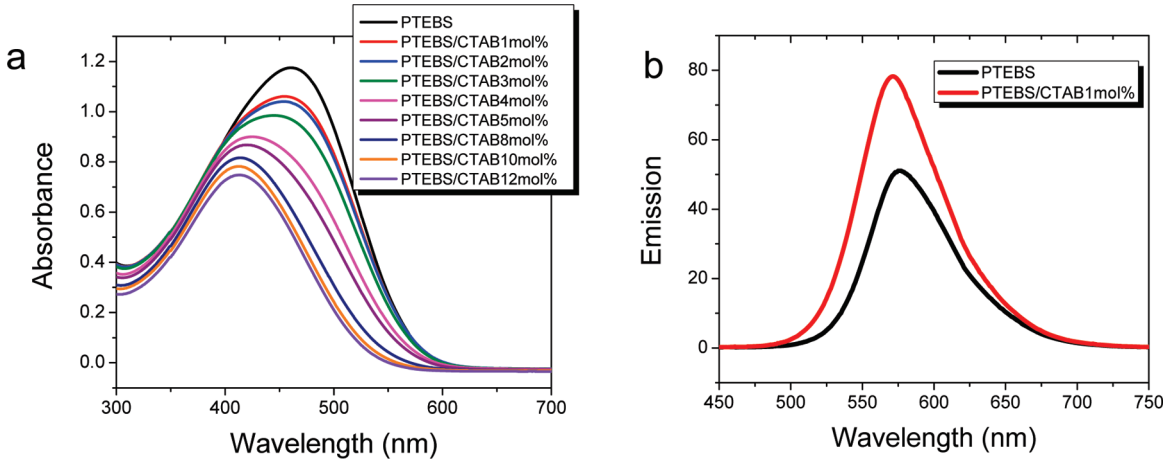

Figure 2. (a) Absorption spectra of PTEBS in the aqueous solution (1×10^{-4} M) by adding amounts (mol %) of CTAB aqueous solution. (b) Fluorescence spectra of PTEBS in the aqueous solution (1×10^{-4} M) excited at 400 nm by adding 1 mol % CTAB.

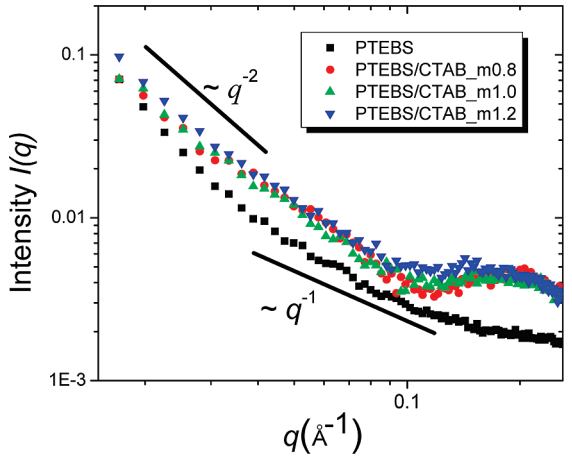

Figure 3. Room temperature SAXS profiles of the PTEBS aqueous solution (~4.5 wt %) and as-prepared PTEBS-CTAB gels with different CTAB:PTEBS molar ratios.

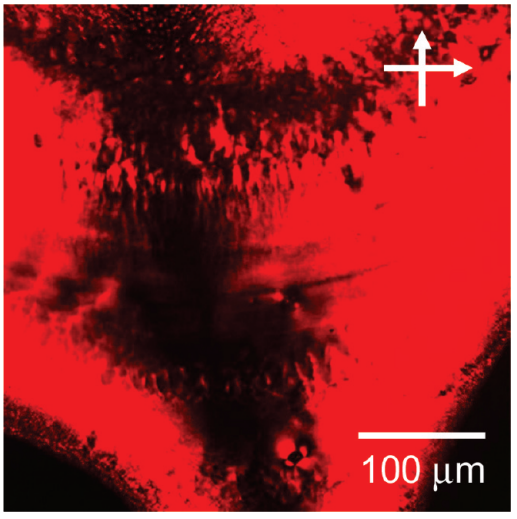

Figure 4. Optical micrograph of the lyotropic gel of the PTEBS-CTAB complex under cross polars.

The ionic bonding of PTEBS-CTAB complexes was further confirmed by FTIR data (Supporting Information Figure 1). Significant changes of vibration bands in the ranges of 1000−1300 cm^{-1} (sulfonate groups) and of 2800−3000 cm^{-1} (methylene groups) were observed. In addition, the vibration peaks of methylene groups in the complex are much narrower compared to those in the PTEBS. This is attributed to the ordered methylene structures in the complex.[54]

The "as-prepared" hydrogel has a concentration of ~4.5 wt % and is optically isotropic with a viscous jellylike consistency. The characterization of the frequency dependent shear modulus is available in the Supporting Information (Supporting Figure 2). The structure in solution is deduced from SAXS data, as shown in Figure 3. A typical scenario for conjugated polymers in solution involves a display of sheet-like scattering with $I(q) \sim q^{-2}$ at low q (long length scales), and rod-like scattering with $I(q) \sim q^{-1}$ at high q (shorter length scales). The scattering at low q is due to side−side association of the polymer backbones into lamellar sheet, whereas at high q the rod-like nature of the polymer chain is evident.[27,34,55] The neat PTEBS as well as all complexes studied reflect this generic scenario, with a gradual rather than sharp transition between −2 and −1 scaling. While it appears that the crossover for the complexes occurs at smaller q, suggestive of increased chain extension in the complexes, the strong distinction between the complexes and the neat PTEBS is found at higher q.

In the high-q region of $q > 0.1$ $Å^{-1}$, the complex exhibits a wide Bragg reflection peak at $q \sim 0.2$ $Å^{-1}$ corresponding to $d \sim 30$ Å. The peak strength and position are weakly dependent on the CTAB:PTEBS molar ratio. This feature is due to weak positional correlations between polymer backbones spaced by the alkyl side chains. The length scale is consistent with a bilayer constructed from disordered chains of the bound CTAB and existing butyl sulfonate groups, as opposed to fully extended or crystallized chains. Similar Bragg scattering has also been observed in other systems, for example recently in a poly(fluorene) conjugated electrolyte complexed with zwitterionic surfactant.[56]

Concentration of the gel by slow evaporation of water produces strongly birefringent samples as shown in Figure 4, indicative of the formation of a lyotropic liquid crystalline phase. By contrast, neat PTEBS does not display any birefringence at these concentrations. The critical concentration for the isotropic-LC transition is $c^* \sim 35$ wt %. Figure 5 shows SAXS data from 70 wt % gels of different CTAB:PTEBS molar ratios, m. The gels all displayed two scattering peaks. For example, the primary and higher order peaks at $q \sim 0.137$ and 0.237 $Å^{-1}$, respectively, are obvious in the gel with $m = 0.8$. Although there are small scale changes in the position and intensity of the peaks, in all three cases, the peaks occur at a ratio of q-vectors of $1:\sqrt{3}$, which is characteristic for hexagonally packed structures. Recently, we

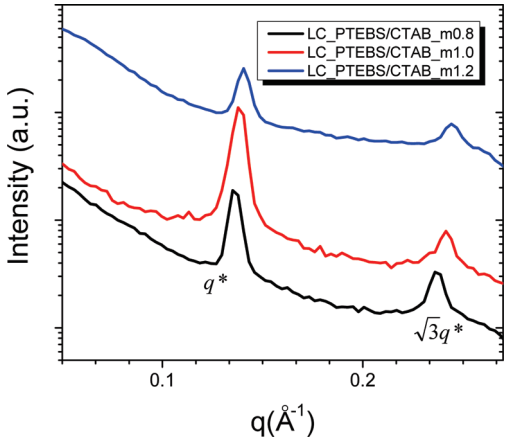

Figure 5. Room temperature SAXS patterns of the lyotropic gels of the PTEBS-CTAB complexes with different CTAB:PTEBS molar ratios. The concentration of the gels is ~70 wt %. Angular position of the higher ordered peak with respect to the first-order maximum is labeled.

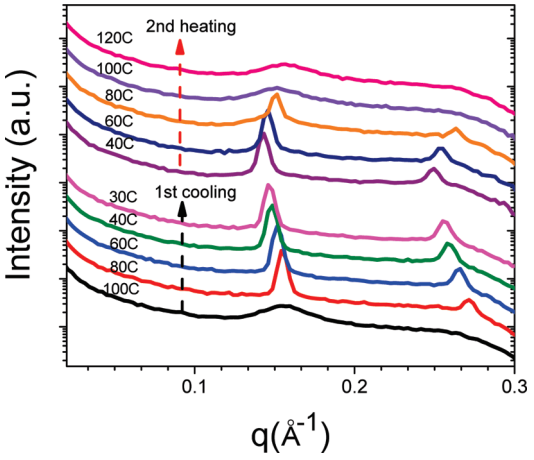

Figure 6. In situ SAXS profiles of the lyotropic gel of the PTEBS-CTAB complex during 1st cooling and 2nd heating cycles. The concentration of the gel is ~90 wt %.

have performed scattering experiments using a different configuration (extended sample holder) to allow access to higher q-space. The new scattering data is again consistent with hexagonal ordering, with two additional higher order peaks clearly shown (Supporting Information Figure 3). The primary Bragg reflection occurred at a d-spacing of $d_0 = 2\pi/q_{max} = 46$ Å and is due to regular positional correlations among individual polymer backbones or small bundles thereof, analogous to structures typically observed in thermotropic systems. The interpolymer distance is given by $d_0(4/3)^{1/2} = 53$ Å which suggests that the alkyl chains of the CTAB are well extended, relative to their conformation in the dilute regime. To the best of our knowledge, this represents the first observation of the hexagonal or columnar phase in the hairy-rod conjugated polymer solutions.

In general, nematic and lamellar phases are predominant in conjugated polymers with shorter side chains whereas the hexagonal columnar phase is predicted to develop stability with respect to the nematic and lamellar phases for polymers with longer side chains. The critical side chain length for phase transitions is dependent on the side chain-backbone interactions as well as their interactions with the solvent. In addition, the lyotropic columnar phase is stabilized by geometrical frustrations such as helical twists, polydispersity and rod flexibility.[31−33] The observation of the lyotropic hexagonal columnar phase in this work is attributed to the presence of the long CTAB side chains as well as the molecular weight polydispersity of the PTEBS backbone. By comparison, complexes prepared at the same equimolar stoichiometry but using shorter C_6 side chains of hexyltrimethylammonium bromide (HTAB) showed only nematic ordering in the concentrated regime above 60 wt %.

Self-assembly in oppositely charged polymer surfactant systems has been well studied both in dilute and concentrated solutions. Prior work has documented for example the lowering of surfactant critical micelle concentration (CMC) and the formation of pearl necklace structures in dilute solutions as well reviewed.[57−59] More complex phase behavior is found in concentrated solutions where biphasic regimes are encountered along with a display of concentration dependent cubic, hexagonal and lamellar phases.[60,61] In the present work, the CTAB content at the critical concentration ($c^* \sim 35$ wt %) of the 1:1 PTEBS-CTAB complex for the hexagonal phase is ~18 wt %, which is lower than that (~25 wt %) of pure CTAB in water for forming a hexagonal columnar phase.[62] Moreover, the d-spacing of the hexagonal columnar phase in the binary CTAB/water system at this concentration is ~63 Å.[62] Increasing concentration of the binary CTAB/water system up to 75 wt % makes the d-spacing decrease down to ~50 Å. This demonstrates that the hexagonal phase observed in the PTEBS-CTAB gel is not due to an independent self-assembly of uncomplexed CTAB in worm-like micelles. We interpret our results as due to lyotropic self-assembly of a hairy-rod species formed by the complexation of CTAB chains with the polymer backbone, rather than the decoration of CTAB worm-like micelles by the oppositely charged polymer chain.

Temperature dependent SAXS was performed to determine the order−disorder transition for the gels. Figure 6 shows SAXS data from a 90 wt % lyotropic solution of the stoichiometric complex at different temperatures obtained during cooling and subsequent heating, after an initial heating ramp. The cooling and heating data show good consistency demonstrating that the transition is fully reversible. On the basis of the room-temperature structural analysis, hexagonal columnar packing of the lyotropic phase is identified. During heating, the scattering peak positions of the first and second order maxima shift slightly toward higher q values, indicating the d-spacing of the cylindrical domains reduces, consistent with the gradual homogenization of the system and thermal mitigation of the interaction potential. The order−disorder transition occurs between 80 and 100 °C and is marked by the disappearance of the second order Bragg peak and the reduction of the primary reflection to a broad correlation halo around $q \sim 0.155$ Å^{-1}. This phenomenon represents the characteristic transition of the ordered liquid crystalline phase to a disordered isotropic liquid state with weak nearest neighbor correlations.[63]

Liquid crystalline materials are in general strongly susceptible to external fields such as shear flow. Oriented films of the lyotropic gels were obtained by simple manual shearing of the samples between glass slides. Figure 7a shows a typical 2-D SAXS pattern of an oriented gel film composed of the 70 wt % stoichiometric complex, with the X-ray beam incident perpendicular to the direction of the previously imposed shear. A pair of strong scattering arcs are present on the equatorial line (with respect to the shear direction) with the second order reflection for the hexagonal structure visible at higher q. From the orthogonal relationship of the scattering vector to the shear, we can infer that the polymer chains are aligned along the shear direction. The alignment of the lyotropic phase is also supported by optical micrographs taken under crossed polarizers. As shown in Figure 7b, a banded texture after mechanical shearing is observed. The polymer backbone is perpendicular to the bands.

Complete removal of water results in the formation of a crystalline material, as evidenced by strong Bragg reflections in

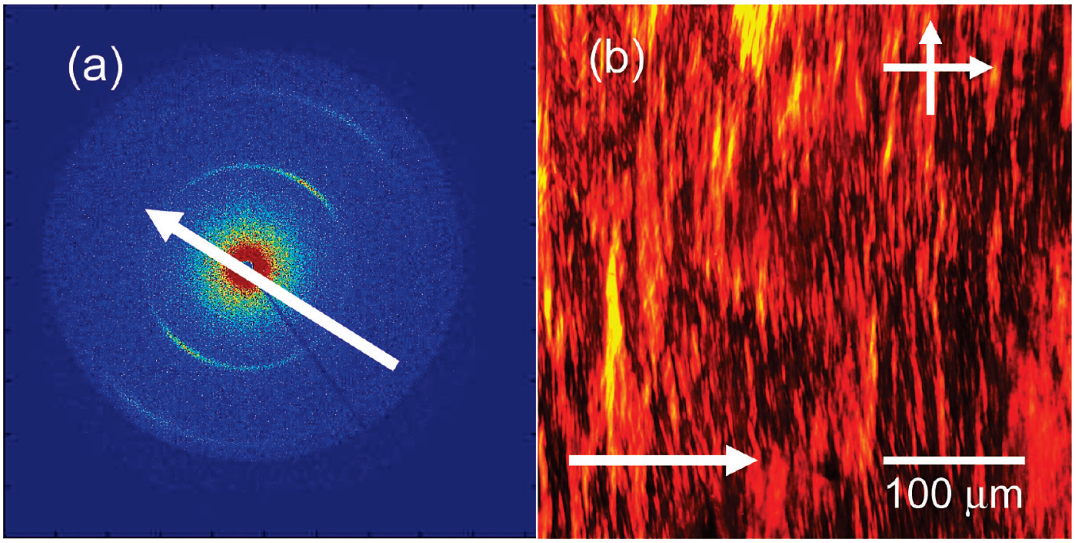

Figure 7. (a) 2D-SAXS fiber pattern and (b) optical micrograph with cross-polars of the lyotropic gel of the PTEBS-CTAB complex after mechanical shearing. Arrows show the shearing direction.

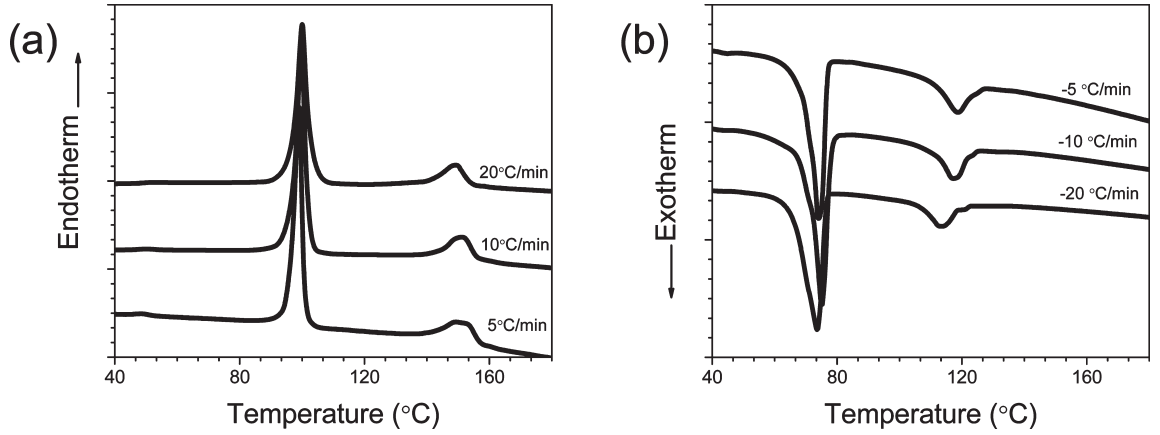

Figure 8. DSC heating and cooling curves at different scanning rates for the dried gel of the PTEBS-CTAB complex.

the wide-angle regime (Supporting Information Figure 4). Heating the dried gel leads to a series of phase transitions through crystalline and ordered liquid crystalline phases. Figure 8 shows a series of DSC heating and cooling curves obtained at different scanning rates for the dried stoichiometric gels. For all the scanning rates, two phase transitions are observed at $T_1 \sim 100$ °C and $T_2 \sim 150$ °C, respectively. They correspond to crystal-to-crystal transition and crystal-to- liquid crystal transition, which is further supported by optical textures and SAXS data. The dried gel is a weakly birefringent viscous fluid when heated to 180 °C under crossed-polarizers in the optical microscope (Supporting Information Figure 5a). Full clearing to the isotropic phase occurred at temperatures in excess of 250 °C. Observations in this regime were limited in order to avoid any thermal degradation of the polymer. The optical texture at 180 °C shows a typical batonnets-like structure (Supporting Information Figure 5a), which is characteristic of ordered liquid crystalline phase. Spherulites develop on cooling to 100 °C as the system crystallizes (Supporting Information Figure 5b). Further cooling resulted in little change of the optical texture.

Figure 9 shows the SAXS patterns of the dried gel of the stoichiometric complex at different temperatures obtained during cooling and subsequent heating, after an initial heating ramp. The heating and cooling data show good reversibility. At room temperature, reflections are present at $q \sim 0.23$ Å^{-1} and $q \sim 0.27$ Å^{-1}. On heating, the first significant change occurs near 90 °C where a new reflection emerges at $q \sim 0.18$ Å^{-1}. The intensity of this peak increases slightly and the position shifts toward lower q with further heating, consistent with simple thermal expansion of the sample. At 150 °C, the intensity of this peak increases markedly, accompanied by a receding of the peak at 0.23 Å^{-1}. The primary reflection at 0.18 Å^{-1} continues to shift to slightly lower q values on heating to 170 °C, again consistent with thermal expansion, but the changes to the scattering are minimal and no further phase transitions are discernible. At high temperature there appears to be a very weak peak at $q \sim 0.13$ Å^{-1}. The origin of this faint signal is currently unknown. One possibility is that it occurs due to thermally driven periodic undulations of the lamellar surface, as observed in prior studies of polyelectrolyte−surfactant complexes.[64] While it is not possible to unambiguously index the crystalline structure of the complex on the basis of these scattering data alone, they do point to a well-defined and reversible phase behavior in which the system transitions between various crystalline and liquid crystalline structures. The scattering data are in good agreement with observations from DSC and POM, and support a crystal−crystal transition near 100 °C and a crystal−liquid crystal transition near 150 °C.

On the basis of POM, SAXS, and DSC, an experimentally determined phase diagram of the PTEBS-CTAB stoichiometric

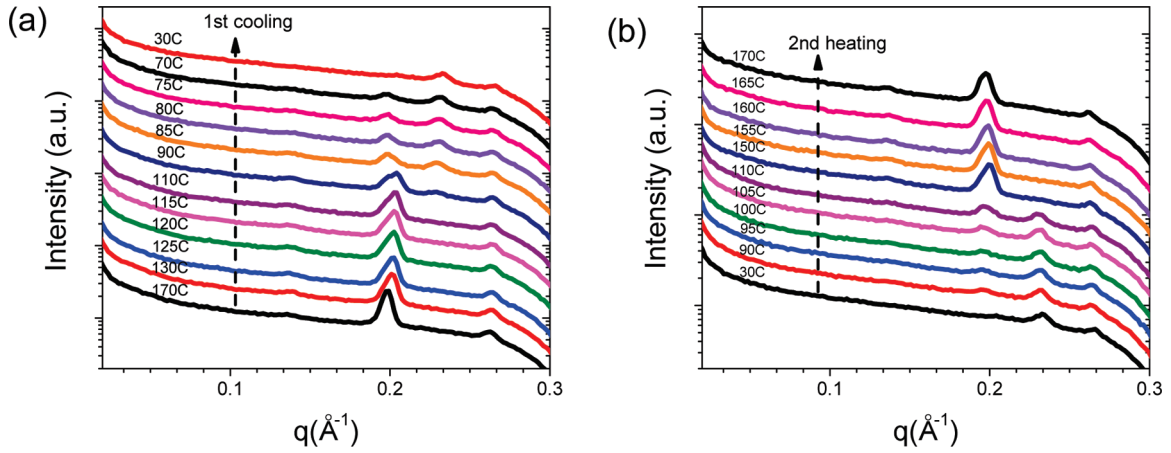

Figure 9. In situ SAXS profiles of the dried gel of the PTEBS-CTAB complex during 1st cooling and 2nd heating cycles.

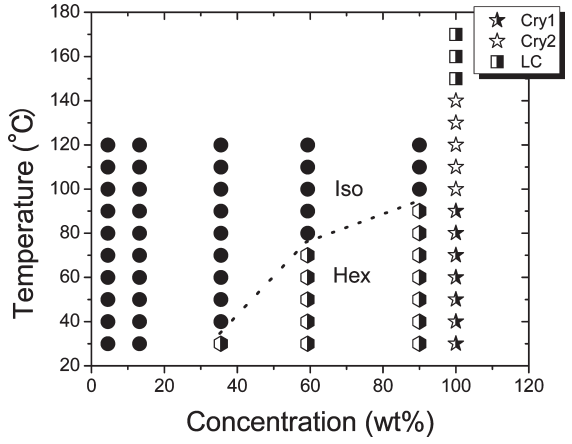

Figure 10. Phase diagram of the gel of the PTEBS-CTAB complex as functions of concentration and temperature.

complex as functions of solution concentration and temperature is constructed as shown in Figure 10. This phase diagram clearly illustrates that hexagonal columnar phases occur and are stable in the concentrated solutions. The critical concentration at room temperature for forming the hexagonal columnar phase is $c^* \sim 35$ wt %. In the lyotropic liquid crystalline phase, the ODT temperature increases with increasing the solution concentration. No lyotropic nematic phase develops in the system. The hexagonal columnar phase exists at room temperature with concentration $c \geq 35$ wt % until the gel is dried completely. The dried gel shows two different crystalline phases and an ordered liquid crystalline phase as a function of increasing temperature.

Conclusions

We have studied the phase behavior of solutions and ordered gels formed by hairy-rod supramolecules of conjugated polymers, PTEBS-CTAB, in water. Removal of water causes dilute optically isotropic solutions to transition to liquid crystalline birefringent phases at room temperature. We have shown via SAXS that the liquid crystalline phase possesses hexagonal symmetry for the three different molar ratios of complexes studied. Under mechanical shearing in the lyotropic phase, the gel can be processed into thin films with polymer chains aligned along the shearing direction. Increasing temperature results in a hexagonal-to-isotropic, order−disorder transition. Upon drying, crystalline phases develop. A full experimental phase diagram as functions of concentration and temperature has been built up.

The potential role of conjugated polymers in energy-related applications means that there requires emergent processing technologies in the cause of high energy conversion efficiency. The use of oriented conjugated polymers in electro-optic devices can enhance device performance, for example through more efficient charge transport or decreased quenching of optical emissions. Lyotropic columnar phases represent a promising starting point for the production of highly aligned thin films by solution-based processing. Our results appear to be the first realization of hexagonal columnar self-assembly in lyotropic mesophases of conjugated polymers and may open up new avenues for processing high performance conjugated polymers.

Acknowledgment. The authors thank Ajay Negi for help with rheological characterization, and Manesh Gopinadhan and Pawel Majewski for insightful discussions. This work is supported by the SOLAR program of the National Science Foundation under DMR-0934520.

Supporting Information Available: Figures showing data for FTIR, rheology, SAXS, WAXS, and optical images. This material is available free of charge via the Internet at http://pubs.acs.org.

References and Notes

(1) Wu, H. B.; Ying, L.; Yang, W.; Cao, Y. *Chem. Soc. Rev.* **2009**, *38*, 3391–3400.
(2) Wu, Y. G.; Hao, X. H.; Wu, J. L.; Jin, J.; Ba, X. W. *Macromolecules* **2010**, *43*, 731–738.
(3) Sax, S.; Rugen-Penkalla, N.; Neuhold, A.; Schuh, S.; Zojer, E.; List, E. J. W.; Mullen, K. *Adv. Mater.* **2010**, *22*, 2087.
(4) Saleh, M.; Baumgarten, M.; Mavrinskiy, A.; Schafer, T.; Mullen, K. *Macromolecules* **2009**, *43*, 137–143.
(5) Becerril, H. A.; Miyaki, N.; Tang, M. L.; Mondal, R.; Sun, Y. S.; Mayer, A. C.; Parmer, J. E.; McGehee, M. D.; Bao, Z. A. *J. Mater. Chem.* **2009**, *19*, 591–593.
(6) Zaumseil, J.; Friend, R. H.; Sirringhaus, H. *Nat. Mater.* **2006**, *5* (1), 69–74.
(7) Chua, L. L.; Ho, P. K. H.; Sirringhaus, H.; Friend, R. H. *Adv. Mater.* **2004**, *16*, 1609.
(8) Gunes, S.; Neugebauer, H.; Sariciftci, N. S. *Chem. Rev.* **2007**, *107*, 1324–1338.
(9) Po, R.; Maggini, M.; Camaioni, N. *J. Phys. Chem. C* **2010**, *114*, 695–706.
(10) Dennler, G.; Scharber, M. C.; Brabec, C. J. *Adv. Mater.* **2009**, *21*, 1323–1338.
(11) Mikroyannidis, J. A.; Sharma, G. D.; Sharma, S. S.; Vijay, Y. K. *J. Phys. Chem. C* **2010**, *114*, 1520−1527.
(12) Guo, Z. S.; Pei, J.; Zhou, Z. L.; Zhao, L. H.; Gibson, G.; Lam, S.; Brug, J. *Polymer* **2009**, *50*, 4794–4800.
(13) Hou, J. H.; Chen, H. Y.; Zhang, S. Q.; Yang, Y. *J. Phys. Chem. C* **2009**, *113*, 21202–21207.

(14) Knaapila, M.; Stepanyan, R.; Horsburgh, L. E.; Monkman, A. P.; Serimaa, R.; Ikkala, O.; Subbotin, A.; Torkkeli, M.; ten Brinke, G. *J. Phys. Chem. B* **2003**, *107*, 14199–14203.
(15) Yoon, Y. S.; Park, K. H.; Lee, J. C. *Macromol. Chem. Phys.* **2009**, *210*, 1510–1518.
(16) Treger, J. S.; Ma, V. Y.; Gao, Y.; Wang, C. C.; Wang, H. L.; Johal, M. S. *J. Phys. Chem. B* **2008**, *112*, 760–763.
(17) Stepanyan, R.; Subbotin, A.; Knaapila, M.; Ikkala, O.; ten Brinke, G. *Macromolecules* **2003**, *36*, 3758–3763.
(18) Subbotin, A.; Stepanyan, R.; Knaapila, M.; Ikkala, O.; ten Brinke, G. *Eur. Phys. J. E* **2003**, *12*, 333–345.
(19) Liu, J. Y.; Zhang, R.; Sauve, G.; Kowalewski, T.; McCullough, R. D. *J. Am. Chem. Soc.* **2008**, *130*, 13167–13176.
(20) Chen, S. H.; Conger, B. M.; Mastrangelo, J. C.; Kende, A. S.; Kim, D. U. *Macromolecules* **1998**, *31*, 8051–8057.
(21) Yang, S. H.; Hsu, C. S. *J. Polym. Sci., Part A: Polym. Chem.* **2009**, *47*, 2713–2733.
(22) Hulvat, J. F.; Stupp, S. I. *Adv. Mater.* **2004**, *16*, 589.
(23) Akagi, K. *J. Polym. Sci., Part A: Polym. Chem.* **2009**, *47*, 2463–2485.
(24) McCulloch, I.; Heeney, M.; Bailey, C.; Genevicius, K.; Macdonald, I.; Shkunov, M.; Sparrowe, D.; Tierney, S.; Wagner, R.; Zhang, W. M.; Chabinyc, M. L.; Kline, R. J.; McGehee, M. D.; Toney, M. F. *Nat. Mater.* **2006**, *5*, 328–333.
(25) Wu, Y. O.; Liu, P.; Ong, B. S.; Srikumar, T.; Zhao, N.; Botton, G.; Zhu, S. P. *Appl. Phys. Lett.* **2005**, *86*, 142102.
(26) Ballauff, M. *Macromolecules* **1986**, *19*, 1366–1374.
(27) Li, Y. C.; Chen, C. Y.; Chang, Y. X.; Chuang, P. Y.; Chen, J. H.; Chen, H. L.; Hsu, C. S.; Ivanov, V. A.; Khalatur, P. G.; Chen, S. A. *Langmuir* **2009**, *25*, 4668–4677.
(28) Koppe, M.; Brabec, C. J.; Heiml, S.; Schausberger, A.; Duffy, W.; Heeney, M.; McCulloch, I. *Macromolecules* **2009**, *42*, 4661–4666.
(29) Alcazar, D.; Wang, F.; Swager, T. M.; Thomas, E. L. *Macromolecules* **2008**, *41*, 9863–9868.
(30) Malik, S.; Jana, T.; Nandi, A. K. *Macromolecules* **2001**, *34*, 275–282.
(31) Selinger, J. V.; Bruinsma, R. F. *Phys. Rev. A* **1991**, *43*, 2922–2931.
(32) Selinger, J. V.; Bruinsma, R. F. *Phys. Rev. A* **1991**, *43*, 2910–2921.
(33) Bohle, A. M.; Holyst, R.; Vilgis, T. *Phys. Rev. Lett.* **1996**, *76*, 1396–1399.
(34) Knaapila, M.; Stepanyan, R.; Torkkeli, M.; Garamus, V. M.; Galbrecht, F.; Nehls, B. S.; Preis, E.; Scherf, U.; Monkman, A. P. *Phys. Rev. E* **2008**, *77*, 051803.
(35) Harre, K.; Wegner, G. *Polymer* **2006**, *47* (20), 7312–7317.
(36) Hamaguchi, M.; Yoshino, K. *Jpn. J. Appl. Phys., Part 2: Lett.* **1994**, *33*, L1689–L1692.
(37) Wang, W.; Lieser, G.; Wegner, G. *Makromol. Chem.—Macromol. Chem. Phys.* **1993**, *194*, 1289–1297.
(38) Bunz, U. H. F. *Chem. Rev.* **2000**, *100*, 1605–1644.
(39) Zhu, Z. G.; Swager, T. M. *J. Am. Chem. Soc.* **2002**, *124*, 9670–9671.
(40) Knaapila, M.; Stepanyan, R.; Lyons, B. P.; Torkkeli, M.; Monkman, A. P. *Adv. Funct. Mater.* **2006**, *16*, 599–609.
(41) Grell, M.; Bradley, D. D. C.; Ungar, G.; Hill, J.; Whitehead, K. S. *Macromolecules* **1999**, *32*, 5810–5817.
(42) Zheng, Z. J.; Yim, K. H.; Saifullah, M. S. M.; Welland, M. E.; Friend, R. H.; Kim, J. S.; Huck, W. T. S. *Nano Lett.* **2007**, *7*, 987–992.
(43) Sirringhaus, H.; Wilson, R. J.; Friend, R. H.; Inbasekaran, M.; Wu, W.; Woo, E. P.; Grell, M.; Bradley, D. D. C. *Appl. Phys. Lett.* **2000**, *77*, 406–408.
(44) Qiao, Q. Q.; McLeskey, J. T. *Appl. Phys. Lett.* **2005**, *86* (15), 153501.
(45) Conio, G.; Bianchi, E.; Ciferri, A.; Krigbaum, W. R. *Macromolecules* **1984**, *17*, 856–861.
(46) Aharoni, S. M.; Walsh, E. K. *Macromolecules* **1979**, *12*, 271–276.
(47) Zhang, S. J.; Kumar, S. *Small* **2008**, *4*, 1270–1283.
(48) Zhang, S. J.; Kinloch, I. A.; Windle, A. H. *Nano Lett.* **2006**, *6*, 568–572.
(49) Rai, P. K.; Pinnick, R. A.; Parra-Vasquez, A. N. G.; Davis, V. A.; Schmidt, H. K.; Hauge, R. H.; Smalley, R. E.; Pasquali, M. *J. Am. Chem. Soc.* **2006**, *128*, 591–595.
(50) Lopez-Cabarcos, E.; Retama, J. R.; Sholin, V.; Carter, S. A. *Polym. Int.* **2007**, *56*, 588–592.
(51) Knaapila, M.; Almasy, L.; Garamus, V. M.; Pearson, C.; Pradhan, S.; Petty, M. C.; Scherf, U.; Burrows, H. D.; Monkman, A. P. *J. Phys. Chem. B* **2006**, *110*, 10248–10257.
(52) Burrows, H. D.; Tapia, M. J.; Fonseca, S. M.; Valente, A. J. M.; Lobo, V. M. M.; Justino, L. L. G.; Qiu, S.; Pradhan, S.; Scherf, U.; Chattopadhyay, N.; Knaapila, M.; Garamus, V. M. *ACS Appl. Mater. Interfaces* **2009**, *1*, 864–874.
(53) Tapia, M. J.; Burrows, H. D.; Knaapila, M.; Monkman, A. P.; Arroyo, A.; Pradhan, S.; Scherf, U.; Pinazo, A.; Perez, L.; Moran, C. *Langmuir* **2006**, *22*, 10170–10174.
(54) Viinikanoja, A.; Areva, S.; Kocharova, N.; Aaritalo, T.; Vuorinen, M.; Savunen, A.; Kankare, J.; Lukkari, J. *Langmuir* **2006**, *22*, 6078–6086.
(55) Knaapila, M.; Almasy, L.; Garamus, V. M.; Ramos, M. L.; Justino, L. L. G.; Galbrecht, F.; Preis, E.; Scherf, U.; Burrows, H. D.; Monkman, A. P. *Polymer* **2008**, *49*, 2033–2038.
(56) Pace, G.; Tu, G.; Fratini, E.; Massip, S.; Huck, W. T. S.; Baglioni, P.; Friend, R. H. *Adv. Mater.* **2010**, *22*, 2073.
(57) Kogej, K. *Adv. Colloid Interface Sci.* **2010**, *158* (1−2), 68–83.
(58) Kwak, J. C., *Polymer-Surfactant Systems*; Marcel Dekker: New York, 1998.
(59) Tam, K. C.; Wyn-Jones, E. *Chem. Soc. Rev.* **2006**, *35*, 693–709.
(60) Ilekti, P.; Martin, T.; Cabane, B.; Piculell, L. *J. Phys. Chem. B* **1999**, *103*, 9831–9840.
(61) Svensson, A.; Piculell, L.; Cabane, B.; Ilekti, P. *J. Phys. Chem. B* **2002**, *106*, 1013–1018.
(62) Ben-David, O.; Nativ-Roth, E.; Yerushalmi-Rozen, R.; Gottlieb, M. *Soft Matter* **2009**, *5*, 1925–1930.
(63) Chai, C. P.; Zhu, X. Q.; Wang, P.; Ren, M. Q.; Chen, X. F.; Xu, Y. D.; Fan, X. H.; Ye, C.; Chen, E. Q.; Zhou, Q. F. *Macromolecules* **2007**, *40*, 9361–9370.
(64) Thunemann, A. F.; Ruppelt, D. *Langmuir* **2001**, *17*, 5098–5102.